

Article

Fabrication of Mg-Doped Sargassum Biochar for Phosphate and Ammonium Recovery

Ye-Eun Lee , Yoonah Jeong, Dong-Chul Shin, Kwang-Ho Ahn , Jin-Hong Jung and I-Tae Kim * 

Department of Environmental Research, Korea Institute of Civil Engineering and Building Technology, Goyang-daero 283, Ilsanseo-gu, Goyang-si 10223, Gyeonggi-do, Korea; yeeunlee@kict.re.kr (Y.-E.L.); yoonahjeong@kict.re.kr (Y.J.); dongchulshin@kict.re.kr (D.-C.S.); khahn@kict.re.kr (K.-H.A.); jinhong98@kict.re.kr (J.-H.J.)

* Correspondence: itkim@kict.re.kr; Tel./Fax: +82-31-910-0885

Abstract: Biochars prepared from macro-algae have a lower C/N ratio compared to lignocellulosic biochar, which is advantageous for direct nutrition. In particular, *Sargassum*, a marine macro-algae, has a high Mg content; hence, it can be expected to adsorb P and N simultaneously. In this study, *Sargassum horneri* biochar (SB), pyrolyzed at 400, 500, and 600 °C, was doped with innate Mg through water leaching, and nutrient recovery from the wastewater-mimicking solution was confirmed. The biochar pyrolyzed at 600 °C showed maximum Mg adsorption during water leaching, and the efficiency of K and Na removal was also high, at 92.7% and 91.9%, respectively. The addition of MgCl₂ during pyrolysis and high ion exchange did not show distinct advantages for surface modification and nutrient adsorption. X-ray photoelectron spectroscopy analysis confirmed the participation of biochar in the surface adsorption of Mg and PO₄ recovery. The PO₄ sorption capacity of biochar reached >120 mg·g⁻¹, while the sorption capacity for NH₄ was low, at 22.8–28.2 mg·g⁻¹, suggesting that Mg-surface-doped SB presented excellent phosphorus recovery. Hence, upgrading an adsorbent as a wastewater-treatment material and soil ameliorant that recovers nutrients using innate Mg from *Sargassum* is possible through appropriate surface modification.

Keywords: phosphate recovery; ammonia recovery; Mg doping; *Sargassum horneri*; algal biochar



Citation: Lee, Y.-E.; Jeong, Y.; Shin, D.-C.; Ahn, K.-H.; Jung, J.-H.; Kim, I.-T. Fabrication of Mg-Doped Sargassum Biochar for Phosphate and Ammonium Recovery. *Sustainability* **2021**, *13*, 12752. <https://doi.org/10.3390/su132212752>

Academic Editors: Petronela Nechita, Rodica-Mihaela Dinică and Bianca Furdui

Received: 29 September 2021
Accepted: 4 November 2021
Published: 18 November 2021

Publisher's Note: MDPI stays neutral with regard to jurisdictional claims in published maps and institutional affiliations.



Copyright: © 2021 by the authors. Licensee MDPI, Basel, Switzerland. This article is an open access article distributed under the terms and conditions of the Creative Commons Attribution (CC BY) license (<https://creativecommons.org/licenses/by/4.0/>).

1. Introduction

Carbon-negative biochars are highly valuable as soil ameliorants because of their nutritional salt-retention ability, resulting from their cation exchange capacity (CEC), and their reduction in nitrogen and carbon emissions to the atmosphere. Various organic wastes are being reproduced as biochars for carbon sequestration and recycling, and studies on biochar production using marine macro-algae have recently drawn attention. Algal biochar has several features that differ from lignocellulosic biochar. For example, the direct nutritive effect of lignocellulosic biochar is small, owing to its high fixed-carbon content [1,2], whereas algal biochar has a low carbon content, a high content of exchangeable minerals, and a high CEC. Hence, algal biochar would be expected to have a direct nutritive effect. Algal biochar with a high CEC is valuable as a biosorbent; therefore, studies on the adsorption and removal of heavy metals [3,4] and phosphorus [5] have also been conducted.

The removal of phosphorus and nitrogen during sewage treatment is a major environmental concern, as eutrophication occurs when nutrients are discharged into the water system above certain concentrations. Chemical treatment is required for the removal of such nutrients because the removal efficiency of biological treatments is limited. Phosphorus and nitrogen need to be recovered as essential nutrients for agricultural use. Nutrient adsorption using Mg has recently attracted attention, complementing phosphorus and nitrogen removal from water systems and agricultural needs [6]. Mg-containing crystals, such as MgNH₄PO₄, increase nutrient retention time, reduce the re-entry of nutrients into water systems, and have high value as fertilizers [7]. Wastewater has a high concentration

of phosphorus and nitrogen but lacks Mg; therefore, an external source such as $MgCl_2$, $Mg(OH)_2$, or MgO is required for nutrient recovery [7–9]. Although biochar is widely used as a soil ameliorant, studies using innate Mg in biomass sources have rarely been conducted. Zheng et al. [10] confirmed that metal-phosphate precipitation due to the negative charge on the biochar surface plays an essential role in ammonium ion adsorption. Zeng et al. [11] performed ammonium and phosphate removal experiments comparing various lignocellulosic biochars and found that the aquatic plant *Thalia dealbata* biochar, which had the highest Mg content, exhibited the highest removal efficiency among the biochars examined. Zhang et al. [12] manufactured surface-modified biochar with MgO and investigated the removal efficiency of only anions, such as phosphate and nitrate. Except for the use of biochar as a seed for $MgNH_4PO_4$ crystal growth, as reported by Muhmood et al. [13], no research has been conducted on the recovery of both P and N using macro-algae biochar as a Mg source.

Sargassum horneri is a brown alga that thrives on the east coast of China and flows into the southern coast of Korea (e.g., Jeju Island), posing a threat to coastal biodiversity [14,15]. The high content of Mg in *Sargassum*, compared with that of lignin biochar, suggests a positive effect on nutrient adsorption [2]. Marine macro-algae containing salt need to be demineralized for utilization as a soil ameliorant. Through prior research, it was confirmed that alkali metals are re-adsorbed, owing to the CEC of biochar, in the processes of pyrolyzing salt-containing raw materials and demineralizing with water. If the surface of *Sargassum* biochar (SB) is modified with innate Mg, which is eluted during the demineralization process, it could then act as a wastewater treatment agent and a high-quality soil fertilizer that recovers phosphorus and nitrogen.

Therefore, in this study, biochar was prepared by pyrolyzing *S. horneri* at 400, 500, and 600 °C, and the possibility of manufacturing MgO -modified biochar was confirmed using the water leaching demineralization method. In addition, the simultaneous removal of phosphate and ammonium ions using modified biochar was confirmed. Finally, the optimized method was verified by comparing the nutrient-adsorption efficiency of three different modification methods in the manufacture of MgO -modified biochar. The results of these studies show that massive amounts of the marine macroalga *S. horneri* can be treated, preventing its potential destruction of coastal ecosystems and providing a potential carbon-negative wastewater-treatment agent. Furthermore, modified *S. horneri* simultaneously demonstrates potential as a high-quality fertilizer, providing recycling alternatives from waste to high-value-added carbon-negative biochar.

2. Materials and Methods

2.1. MgO -Modified Biochar Fabrication

A diagram of the components of the pyrolysis device used in this study is shown in Figure S1 (Supplementary). Naturally dried *S. horneri* was collected from a coastal area of Yeosu (south seaside) in Korea and was ground unwashed. Samples (150.00 g) were pyrolyzed at 400, 500, and 600 °C, respectively, for 1 h in an electric furnace, and the generated biogas was combusted and exhausted. The heating rate was 10 °C/min, and the N_2 gas influx was 2 L/min. N_2 gas was allowed to flow for 10 min before the sample was inserted into the furnace. After pyrolysis, the SB sample was removed from the electric furnace and left to cool in a closed container at room temperature with continuous N_2 purging to prevent any oxidation.

The SB was mixed with distilled water at a 1:10 *w/w* ratio and stirred for 30 min to modify the biochar surface and achieve desalination. In this process, the salt contained in the SB was diluted in water and, owing to CEC, the alkali and alkali earth metal (AAEM) ions eluted from the SB were resorbed onto the biochar surface. Since Mg ion has a relatively higher ionic strength than Na or K ions, its ions are more competitive in this process.

After stirring, Mg-adsorbed surface-modified *S. horneri* biochar (Mg-SB) was separated with saline water using a 47 mm GF/C filter (Whatman) and an electric aspirator (EYELA, model A-1000S, Fisher Scientific, Hampton, NH, USA), and dried for 24 h at 70 °C.

To determine the optimal MgO-impregnation method, pyrolyzed SB was applied to the two other methods. First, 836.6 mg of $MgCl_2$ was dissolved in 100 mL of deionized water, and 200 g of *S. horneri* was immersed in the solution, as described by Zhang et al. [12]. The SB was then dried for 24 h at 70 °C, followed by pyrolyzing at 600 °C for 1 h. The $MgCl_2$ containing biochar ($MgCl_2$ -SB) underwent the same desalination and modification process as described for Mg-SB. The second method was an ion exchange process in which a Mg-SB sample was added to an aqueous solution of 50 ppm Mg, obtained by dissolving 209.15 mg of $MgCl_2$ in 500 mL deionized water. The mixture was stirred for 30 min to allow for the exchange of more AAEM ions without replacing the Mg. Subsequently, the sample was separated and dried for 24 h at 70 °C and labeled as I-Mg-SB.

2.2. Sorption Experiments

Sorption experiments were carried out using NH_4Cl and KH_2PO_4 as sources of ammonium and phosphate, respectively. The ammonium concentration was fixed at 1000 ppm, and the phosphate concentration was 100, 200, 400, or 600 ppm. A total of 5.00 g of SB was added to 1 L of ammonium and phosphate solution, and 3 mL of sample was collected after 10, 30, 60, 100, and 150 min. The pH was not adjusted, but changes in pH were recorded at the beginning of the sorption experiment and at each sample collection time point. After the experiment, the SB was separated using a GF/C filter and aspirator and dried for 24 h at 70 °C.

To determine the optimal MgO-modification method, three different MgO-modified samples were also subjected to sorption experiments. A SB sample (5.00 g) was added to 1 L of a 1000 ppm ammonium and 600 ppm phosphate solution, and 3 mL of sample was collected after 2, 5, 10, 20, and 30 min. The pH was recorded at each time point.

The residual phosphate concentration of each collected solution was measured using a low-range (0.06–5.00 ppm) and high-range (1.00 to 100 ppm) PO_4^{3-} measuring kit (C-mac, Daejun, Korea). The ammonium concentration was measured using the Nessler (HACH Co., Loveland, CO, USA) method and spectrophotometry (DR 5000, HACH Co., Loveland, CO, USA).

2.3. Biochar Characterization

Ultimate analysis of raw and pyrolyzed SB samples was performed using a CHNS/O elemental analyzer (Elementar VARIO EL cube, Elementar Analysensysteme GmbH, Berlin, Germany). To determine the effects of surface modification on the specific surface area, the Brunauer–Emmett–Teller (BET) specific surface area (BELSORP-MAX, BEL Japan Inc., Osaka, Japan) was measured. The AAEM content of biochar changed with the pyrolysis temperatures, and the modification methods were quantified using inductively coupled plasma optical emission spectroscopy (ICP-OES; Agilent 5100, Agilent Technologies, Santa Clara, CA, USA). For nutrient crystallization confirmation, X-ray diffraction (XRD) analysis was performed using a DMAX 2500 diffractometer (Rigaku, Japan). To identify changes in surface chemistry between biochar, Mg, and nutrients, induced by different modification methods, X-ray photoelectron spectroscopy (XPS) measurements were carried out with a K-alpha (Thermo Fisher Scientific, Loughborough, UK).

2.4. Statistical Analysis

Experimental data were statistically analyzed using Microsoft Excel 2016. The mean values and standard deviations of the phosphate and ammonium concentrations in solutions and AAEM concentrations in SB were also calculated.

3. Results and Discussion

3.1. Effect of Pyrolysis Temperature and Modification on *Sargassum* Biochar's Physicochemical Properties

The elemental compositions of the biochars prepared at different pyrolysis temperatures are summarized in Table 1. As the pyrolysis temperature increased, the nitrogen and

oxygen contents decreased, but the carbon content increased. The sulfur content increased up to 500 °C and then sharply decreased at 600 °C. Except for the oxygen and sulfur content, there was no significant difference in the composition between 500 °C and 600 °C. Hence, it can be interpreted that the SB was sufficiently carbonized when pyrolyzed above 500 °C. The carbon and nitrogen ratio also increased from 11.48 to 16.83 as the pyrolysis temperature increased. Lignocellulosic biochar has a high carbon content, a low nitrogen content, and low direct benefits to the nutrient supply [16]. In contrast, a C/N ratio < 20, as in this study for SB, indicates that bioavailable nutrients could be directly contributed to soils from SB [2].

Table 1. Elemental composition of *S. horneri* pyrolyzed biochars (SB) produced at different temperatures.

(Mean wt% ± SD; n = 2)	Ultimate Analysis					
	C	H	N	S	O	C/N
Raw	28.19 ± 0.3	4.51 ± 0.0	2.55 ± 0.0	3.44 ± 4.9	34.22 ± 0.1	11.08 ± 0.3
400 °C SB	38.51 ± 4.6	3.83 ± 0.4	3.36 ± 0.4	6.24 ± 0.5	25.02 ± 0.0	11.48 ± 0.0
500 °C SB	38.13 ± 1.4	3.78 ± 0.2	2.45 ± 0.2	6.78 ± 0.3	20.63 ± 0.4	15.60 ± 0.4
600 °C SB	39.38 ± 0.6	3.78 ± 0.1	2.34 ± 0.2	1.99 ± 2.8	15.59 ± 0.3	16.83 ± 1.4

The pyrolysis yield and modification yield were calculated using Equations (1) and (2):

$$\text{Pyrolysis yield (PY, \%)} = \frac{\text{Mass after pyrolysis}}{\text{Mass of raw sample}} \times 100 \quad (1)$$

$$\text{Modification yield (MY, \%)} = \frac{\text{Mass after modification}}{\text{Mass of biochar sample}} \times 100 \quad (2)$$

The pyrolysis yield decreased with an increase in temperature, but modification caused the yield to vary, owing to NaCl dissolution during the modification process of the biochars (Table 2).

Table 2. Yields of biochars produced at different pyrolysis temperatures and with different modifications.

(Mean wt% ± SD; n = 2)	400 °C	500 °C	600 °C
Pyrolysis yield	60.07 ± 0.7	48.92 ± 1.2	46.08 ± 0.6
Modification yield	58.62 ± 0.9	61.82 ± 3.7	56.19 ± 5.4

Figure 1 shows the change in AAEM (Na, K, Mg, and Ca) contents at different pyrolysis temperatures and modifications per 100 g of raw *S. horneri*. Based on the ICP analysis results, AAEM contents in SB and Mg-SB were calculated as shown, respectively, in Equations (3) and (4):

$$\text{AAEM content of SB (g)} = \text{Mass of raw } S.\text{horneri(g)} \times \left(\frac{\text{PY}(\%)}{100} \right) \times \left(\frac{\text{ICP result}(\%)}{100} \right) \quad (3)$$

$$\text{AAEM content of Mg_SB (g)} = \text{Mass of raw } S.\text{horneri(g)} \times \left(\frac{\text{PY}(\%)}{100} \right) \times \left(\frac{\text{MY}(\%)}{100} \right) \times \left(\frac{\text{ICP result}(\%)}{100} \right) \quad (4)$$

AAEMs contained in raw *S. horneri*, except for Na, were partially volatilized as the pyrolysis temperature increased, whereas Na was hardly volatilized. After water leaching, the Mg-SB sample showed that most of the K and Na contained in raw *S. horneri* was eliminated. The K and Na were removed by 92.63–93.46% and 91.88–94.59%, respectively. The K and Na removal efficiencies decreased slightly as the pyrolysis temperature increased. The influence of the pyrolysis temperature or water leaching modification on the Ca content

was negligible. Only SB pyrolyzed at 400 °C showed a Mg loss of 47.7% after water leaching, and no significant loss was observed at 500 °C and 600 °C.

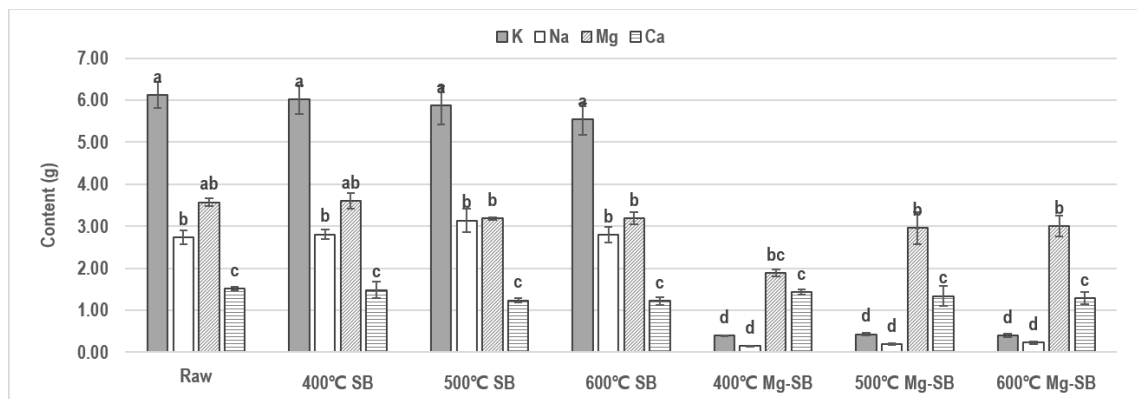


Figure 1. Changes in alkali and alkali earth metal (AAEM; Na, K, Mg, and Ca) contents at different pyrolysis temperatures and different modifications of *S. horneri* char (SB) and Mg-SB (mean g% \pm SD; $n = 2$). Different letters indicate statistically significant difference.

These phenomena could be interpreted as an effect of the CEC of biochar and the structural forms of AAEMs in *S. horneri*. Mainly, K and Na were lost in water leaching, indicating that they existed in the form of water-soluble salts. The amount of Na remained consistent during pyrolysis, but the volatile amount of K increased as the pyrolysis temperature increased. This implies that a more significant fraction of the Na was in a crystallized mineral salt form, capable of enduring high temperatures. In contrast, K was present in an organic salt form that decomposed at high pyrolysis temperatures.

Although at least 47.7% of the Mg contained in SB was in a water-soluble form, it showed high retention after the water leaching of SB pyrolyzed at 500 °C and 600 °C. An increase in the CEC, owing to increased pyrolysis temperatures, stimulated the adsorption of the eluted Mg, caused by water leaching, to the biochar surface. Similarly, this also led to increased residual monovalent ions, which provides evidence of adsorption via cation exchange. These results also indicate that divalent ions have a higher affinity for adsorption to SB than monovalent ions.

The water leaching modification also affected the pore properties of the biochar. Table 3 shows the variations in the BET surface area with pyrolysis temperatures and modifications. Comparing the biochar before and after the modification, the BET increased about 2-fold at 400 °C and 500 °C, and approximately 6-fold at 600 °C. The most significant difference induced by water leaching was salt elimination. KCl and NaCl embedded in the organic material acted as a template, and the pore structure in the material developed after salt dissolution by water leaching [17].

Table 3. Brunauer–Emmett–Teller (BET) surface area of raw *S. horneri* and biochar as a function of the water leaching modification.

	RAW	400 °C SB	500 °C SB	600 °C SB	400 °C Mg-SB	500 °C Mg-SB	600 °C Mg-SB
V_m (cm ³ (STP) g ⁻¹)	0.1042	0.567	1.871	1.8214	1.2907	3.4962	10.647
$a_{s,BET}$ (m ² g ⁻¹)	0.45346	2.4677	8.1435	7.9277	5.6177	15.217	46.342
Total pore volume ($p/p_0 = 0.990$) (cm ³ g ⁻¹)	0.0030	0.0147	0.0517	0.0536	0.0309	0.0883	0.1358
Average pore diameter (nm)	26.043	23.757	25.409	27.037	21.994	23.209	11.723

In PO_4 adsorption, pores larger than 10 nm (mesoporous material) are effective for enhancing adsorption ability [18]. BET analysis using N_2 gas is suitable for the mesoporous distribution analysis, showing that all conditions with an average pore diameter larger than 10 nm were suitable for PO_4 adsorption.

The high Mg content and surface-doping of SB may have a positive effect on atmospheric CO_2 sequestration when the SB is spread on soil. Future studies characterizing the microporous structure of SB and CO_2 adsorption and desorption are needed; such studies would also help inspire research on *S. horneri* recycling. Therefore, our future research will focus on characterizing the effect of SB in capturing and storing CO_2 as well as changes in the nutrient supply when SB is applied to soil.

The XRD results (Figure 2) clearly show the effects of modification. Salt crystals, such as KCl and NaCl, were distinctly present before the water leaching; after water leaching, most of the NaCl and KCl crystal peaks disappeared, and new peaks of MgO, $\text{Mg}(\text{OH})_2$, quartz, and calcite were observed. MgO and $\text{Mg}(\text{OH})_2$ peaks of Mg-SB showed higher intensities at pyrolysis temperatures greater than 400 °C. For marine algae utilization, previous studies have removed the salt prior to pyrolysis. However, the results of the current study show that pyrolysis and subsequent water leaching enhanced not only the salt removal efficiency and the specific surface area, but also the potential for nutrient adsorption due to Mg-doped biochar surface formation.

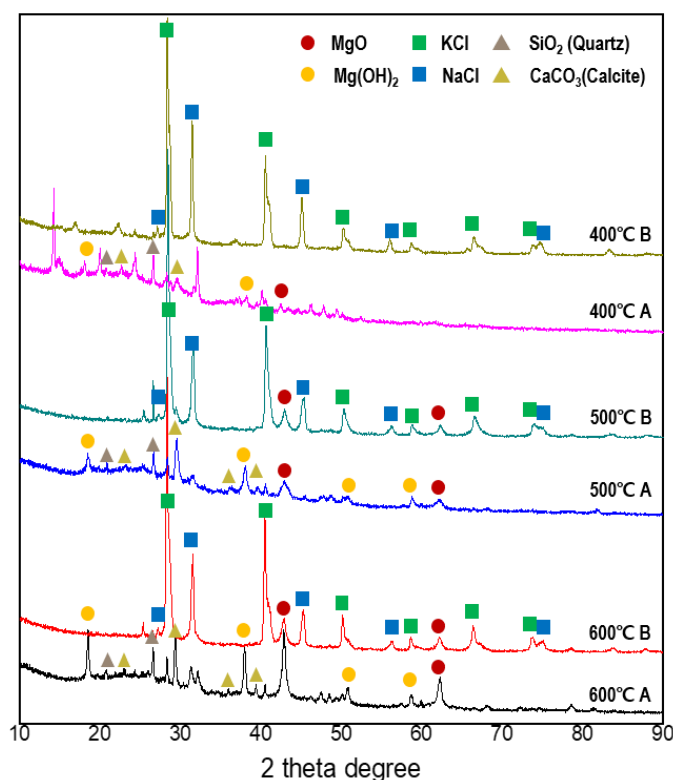


Figure 2. XRD results before (B) and after (A) water leaching modification at each pyrolysis temperature.

3.2. Nutrient Adsorption Capacity of Mg-SB as a Function of Pyrolysis Temperature

Figure 3 shows the results for the removal efficiency and pH change, following the addition of Mg-SB to a mixed solution with a constant ammonium ion concentration of 1000 ppm and varying phosphate concentrations of 100, 200, 400, and 600 ppm, at each pyrolysis temperature. Mg-SB pyrolyzed at 500 °C and 600 °C showed similar trends under all conditions. The removal reached 90% at the lowest phosphate concentration (100 ppm) but increased to 99% as the ion concentration increased from 200 ppm to 600 ppm. The surface of insufficiently Mg-doped SB, pyrolyzed at 400 °C, was characterized by a low CEC, causing a decrease in phosphate ion removal from 90% to 70% as the ion concentration

increased. The ammonium ion removal was relatively low (5–15%) in all conditions, except for the Mg-SB pyrolyzed at 400 °C. SB pyrolyzed at 400 °C had a relatively low CEC and was inefficient with regard to the adsorption of divalent cations but was adequate for ammonium adsorption. If the SB with high CEC, pyrolyzed at 500 °C and 600 °C, adsorbs massive amounts of Mg on the surface, then the lack of active sites would eventually be reflected in a low ammonium adsorption efficiency; hence, the relatively high ammonium adsorption of SB pyrolyzed at 400 °C could be explained. However, further research is needed to understand the lower-than-expected amount of ammonium ions in combination with phosphate and Mg.

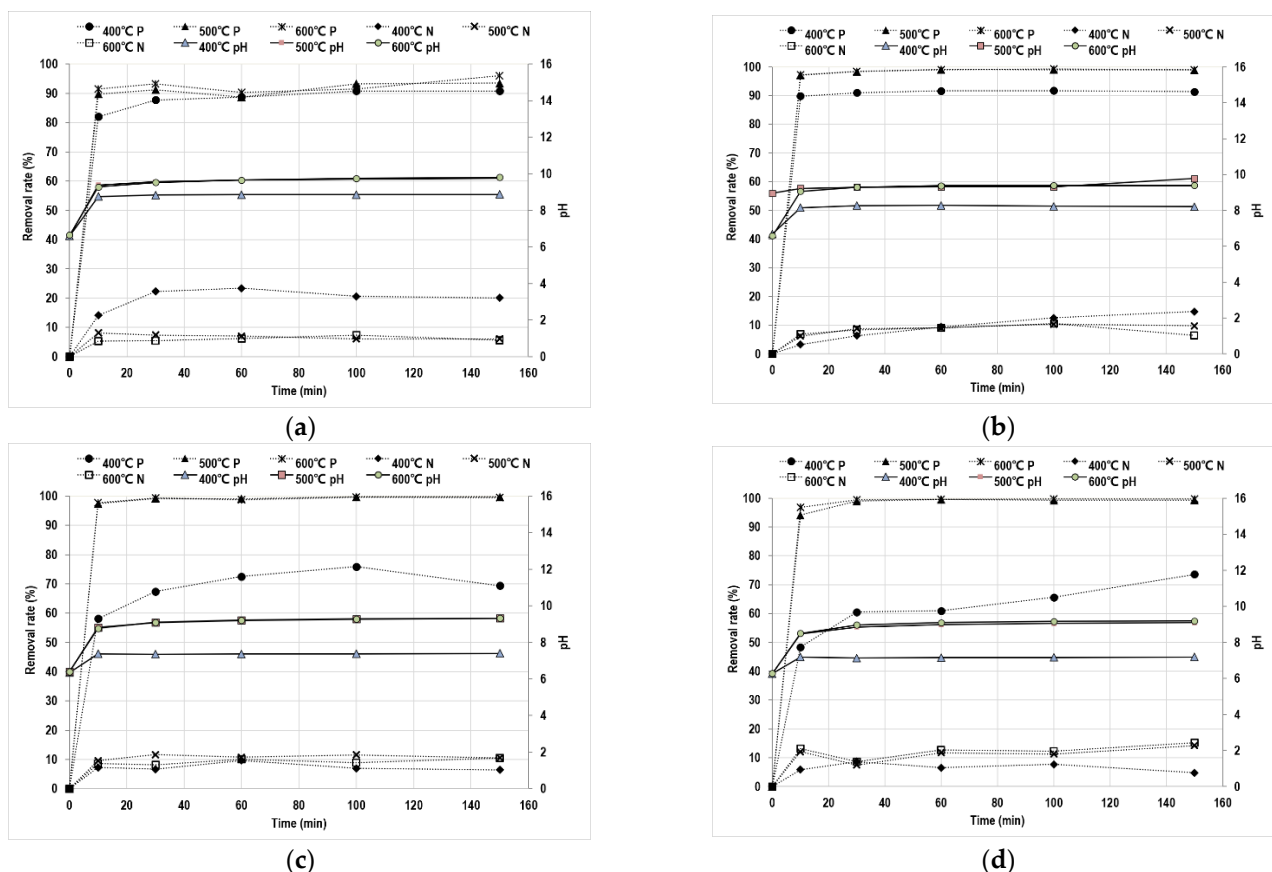


Figure 3. Adsorption test results of Mg-adsorbed surface-modified *S. horneri* biochar (Mg-SB) based on pyrolysis temperature and nutrient concentration. (a) PO₄ 100 ppm, NH₄ 1000 ppm, ($n = 3$, R^2 of pH/PO₄/NH₄: 0.97–0.99/0.97–0.99/0.88–0.99); (b) PO₄ 200 ppm, NH₄ 1000 ppm ($n = 1$), (c) PO₄ 400 ppm, NH₄ 1000 ppm ($n = 1$), (d) PO₄ 600 ppm, NH₄ 1000 ppm ($n = 1$).

The pH of the mixed solution was 6, which is not a suitable environment for MgNH₄PO₄ formation through phosphate and ammonium ion adsorption; the optimum value is a pH of 8 to 11 [19,20]. When MgCl₂ is used as the Mg source, a pH adjuster, such as NaOH, is required. Biochar has a different pH depending on the raw material, but it typically has an average pH of 8.1 [21,22]. In addition, the pH is further increased when the ash content or minerals in the raw material are high or when the pyrolysis temperature is increased [23]. As shown in Figure 3, the pH of all the samples increased after biochar addition, and in the case of Mg-SB pyrolyzed at 500 °C and 600 °C, the pH was maintained in the range of 8 to 10 under all conditions. Thus, Mg-doped biochar contributes to creating a favorable environment without additional chemical input for the nutrient crystallization, which is effective for long-term nutrient retention.

Figure 4 shows SEM images of Mg-SB biochar pyrolyzed at 600 °C after the adsorption test, and the highest elimination efficiency of phosphate and ammonium ions. All conditions showed crystal formation. The amount and size of the crystals increased as the

phosphate ion concentration increased. Crystal formation at the biochar surface makes it valuable as a soil amendment that supplies nutrients continuously in both direct and indirect ways.

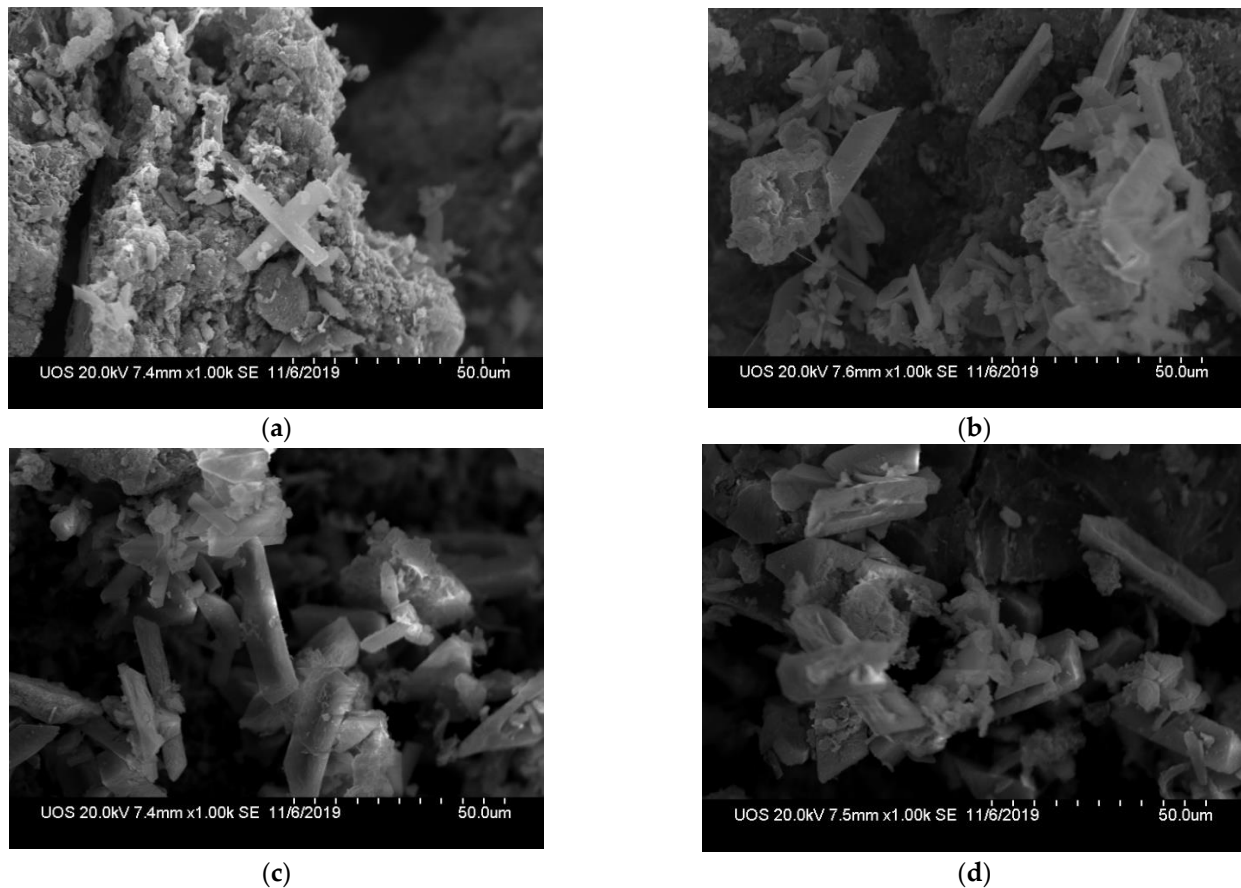


Figure 4. Scanning electron microscopy images of Mg-SB pyrolyzed at 600 °C after the nutrient adsorption test. (a) PO₄ 100 ppm, NH₄ 1000 ppm, (b) PO₄ 200 ppm, NH₄ 1000 ppm, (c) PO₄ 400 ppm, NH₄ 1000 ppm, (d) PO₄ 600 ppm, NH₄ 1000 ppm.

3.3. Nutrient Adsorption as a Function of Different Modification Methods

Different methods, such as water leaching demineralization, ion exchange, and MgCl₂ addition, were compared with the aim to produce the most Mg-enriched biochar. The changes in AAEMs contents are shown in Figure 5. In I-Mg-SB, the content of all of the AAEMs slightly decreased compared to those in the Mg-SB. This result suggests that additional ion exchange after Mg adsorption occurred primarily through water leaching, which did not positively affect Mg adsorption. MgCl₂-SB showed a slightly higher Mg content than that of SB obtained using other methods, but the difference was not significant.

Figure 6 shows the XRD results of the differently modified SBs. The MgO peaks of MgCl₂-Raw and SB were similar, implying that additional MgCl₂ does not contribute to MgO formation during pyrolysis. After water leaching demineralization, the intensity of the MgO peaks increased under all conditions. Salt elimination and exposure to MgO, Mg(OH)₂, quartz, and calcite peaks were in line with previous results (Figure 2). Overall, water leaching demineralization is a significant and effective method for eliminating redundant salts and forming MgO and Mg(OH)₂, rather than ion exchange or Mg-injected pyrolysis.

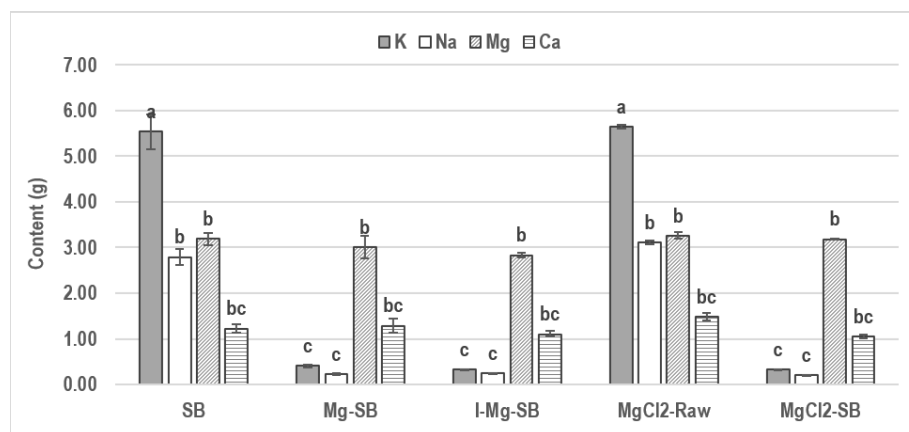


Figure 5. Changes in alkali and alkali earth metal (AAEM; Na, K, Mg, and Ca) content with different modification methods (mean g% \pm SD; $n = 2$). Different letters indicate statistically significant difference.

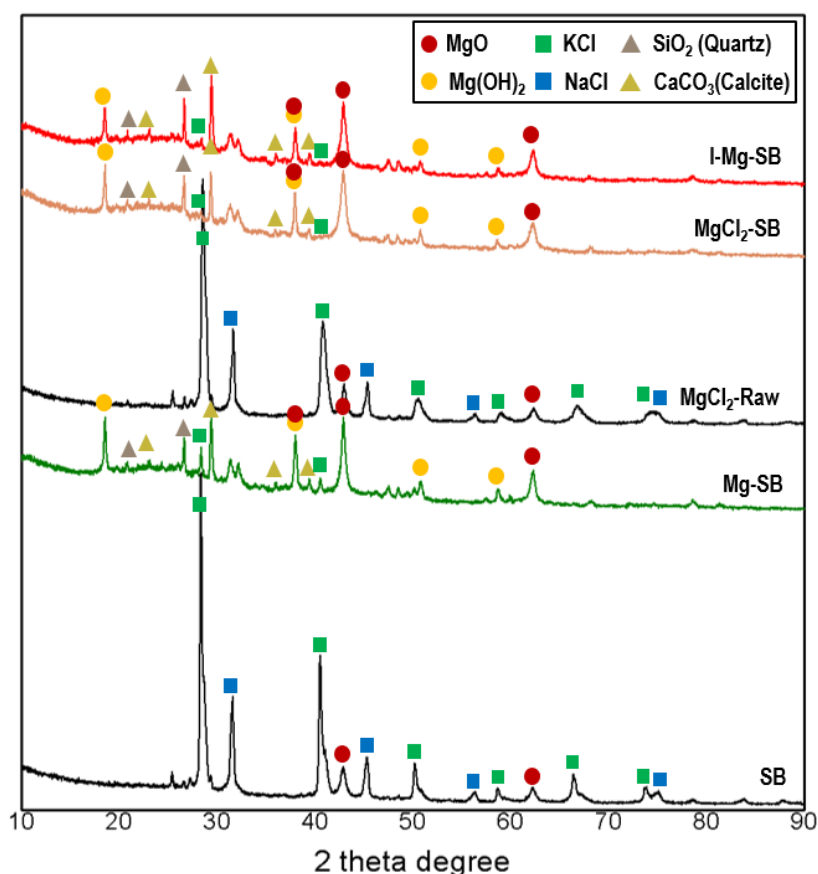


Figure 6. XRD results of SB subjected to different modification methods at a pyrolysis temperature of 600 °C.

Figure 7 shows the results for the phosphate and ammonium ion adsorption test for each modification method, and Figure 8 shows the SEM results before and after the sorption test. The phosphate removal rate of MgCl₂-SB was slower than that of Mg-SB, while I-Mg-SB removed it faster. The final phosphate removal efficiency of Mg-SB and I-Mg-SB was 99% when adsorbed for 20 min, and slightly lower (96%) for MgCl₂-SB when adsorbed for 30 min. The ammonium removal efficiencies were 13.1%, 14.0%, and 11.1% for Mg-SB, I-Mg-SB, and MgCl₂-SB, respectively, which were significantly lower than those for phosphate. Comparing the final removal efficiencies of phosphate and

ammonium ions, I-Mg-SB ranked the highest and MgCl₂-SB the lowest for both NH₄ and PO₄ removal. Although the Mg content of MgCl₂-SB was higher than that of Mg-SB and I-Mg-SB (Figure 5), the removal efficiencies and rates were the lowest, indicating that Mg surface-adsorption by water leaching demineralization is the most effective method for phosphate removal.

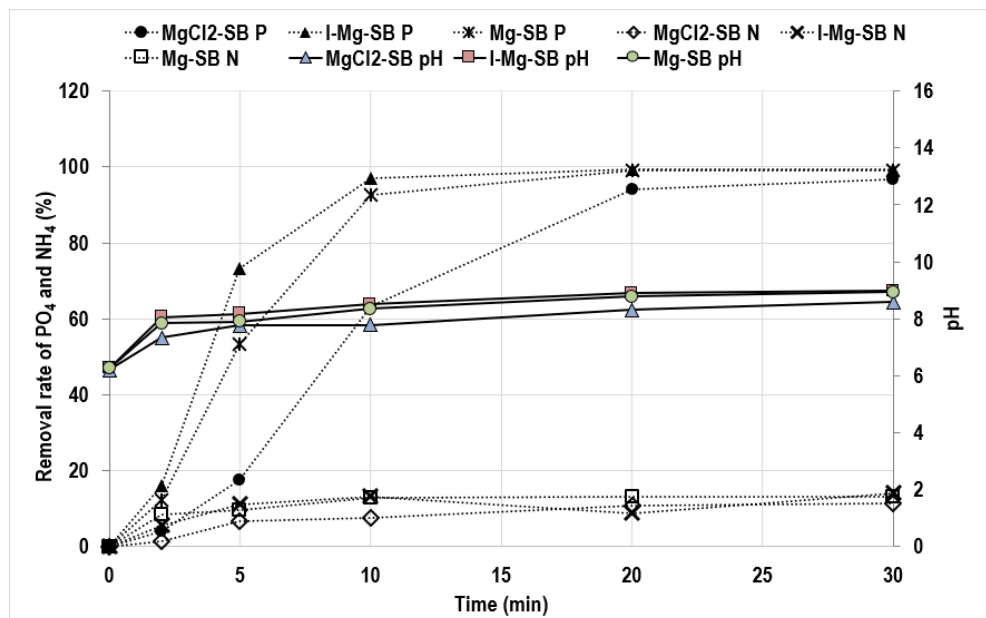


Figure 7. Nutrient adsorption results for Mg-adsorbed surface-modified *S. horneri* biochar (Mg-SB), I-Mg-SB, and MgCl₂-SB with PO₄ 600 ppm or NH₄ 1000 ppm solution ($n = 2$). R² of pH: 0.95–0.99, R² of PO₄: 0.99, R² of NH₄: 0.90–0.98).

3.4. XPS Analysis

Nutrient adsorption and precipitation on the SB surface were further confirmed by XPS analysis to elucidate the water leaching demineralization and adsorption mechanism. The XPS spectra of C1s, N1s, Mg2p, and P2p of SB are shown in Figure 10. The C1s spectra of SB between 280 and 291 eV were deconvoluted into five peaks. The two peaks at 292.8 eV and 295.5 eV of the C1s spectra represent KCl [24]. The peaks of KCl disappeared after water leaching, as in the XRD analysis. Mg sorption could originate from biochar functional groups such as hydroxyl (C-OH) and carboxyl (C-OOH) [25], and π -electron resonance induced by aromatic carbon [26,27]. After the demineralization of SB at 600 °C for MgCl₂-Raw and ion-exchanged I-Mg-SB, the peak of the carboxyl group (-O-C=O) at 289.3 eV and C-O at 286 eV [28,29] increased compared with that of the non-demineralized biochar. The aromatic C=C peak at 284.2 eV shifted to a higher binding energy after the water leaching modification. Mg adsorption onto the biochar surface contributed to these peak intensity changes and peak shifts. After the nutrient sorption test, the intensity-increase of oxygen-containing functional groups and C=C aromatic groups of Mg-SB and I-Mg-SB showed that these functional groups were involved in nutrient adsorption [30]. In contrast, MgCl₂-SB showed insignificant changes in intensity even after the adsorption test. Thus, it can be inferred that the eluted Mg reacts independently with nutrients, and biochar is rarely involved in direct nutrient adsorption.

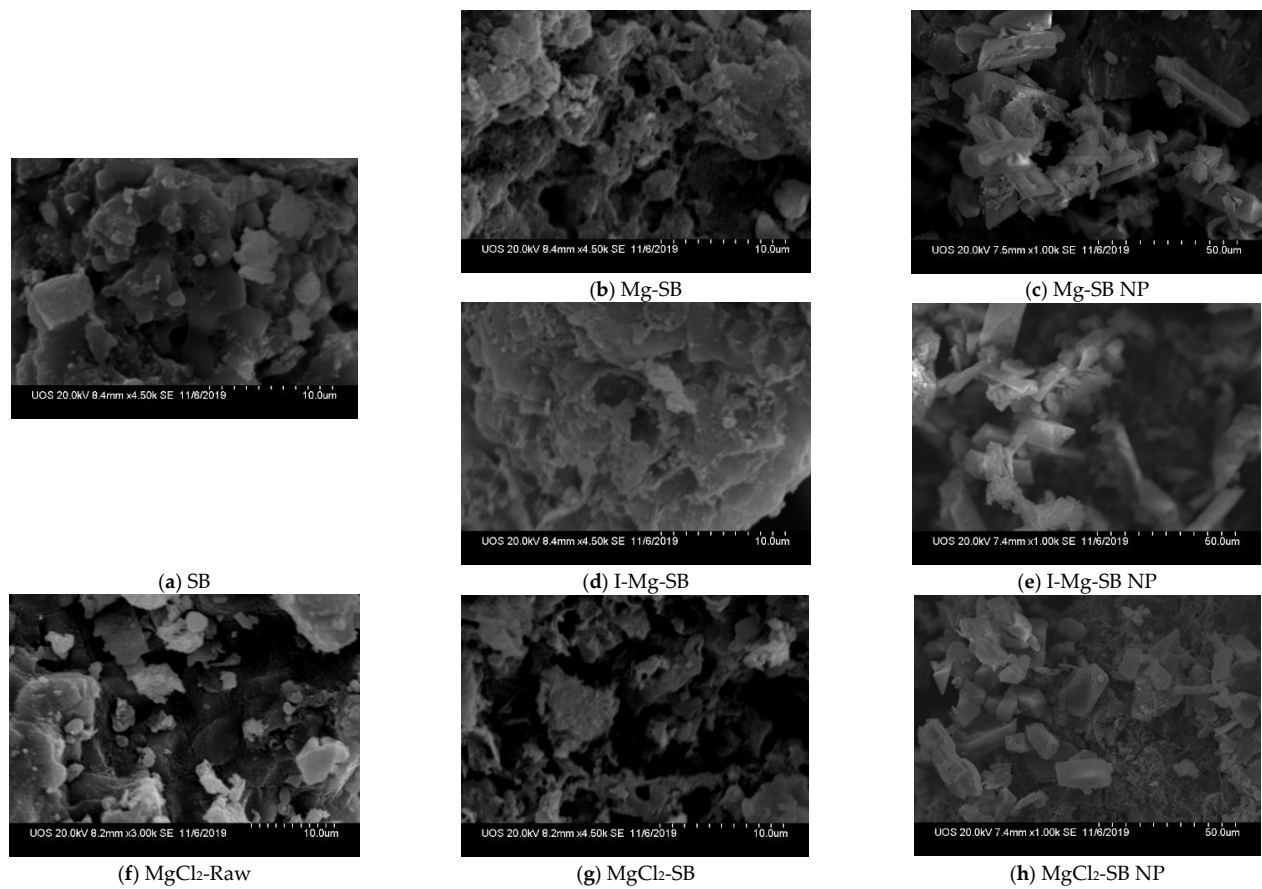


Figure 8. Scanning electron microscopy (SEM) images of SBs before and after the sorption test. Mg-SB, I-Mg-SB, MgCl₂-SB sorption test-(after the NH₄ and PO₄ adsorption: NP, and MgCl₂-Raw: before the water demineralization modification).

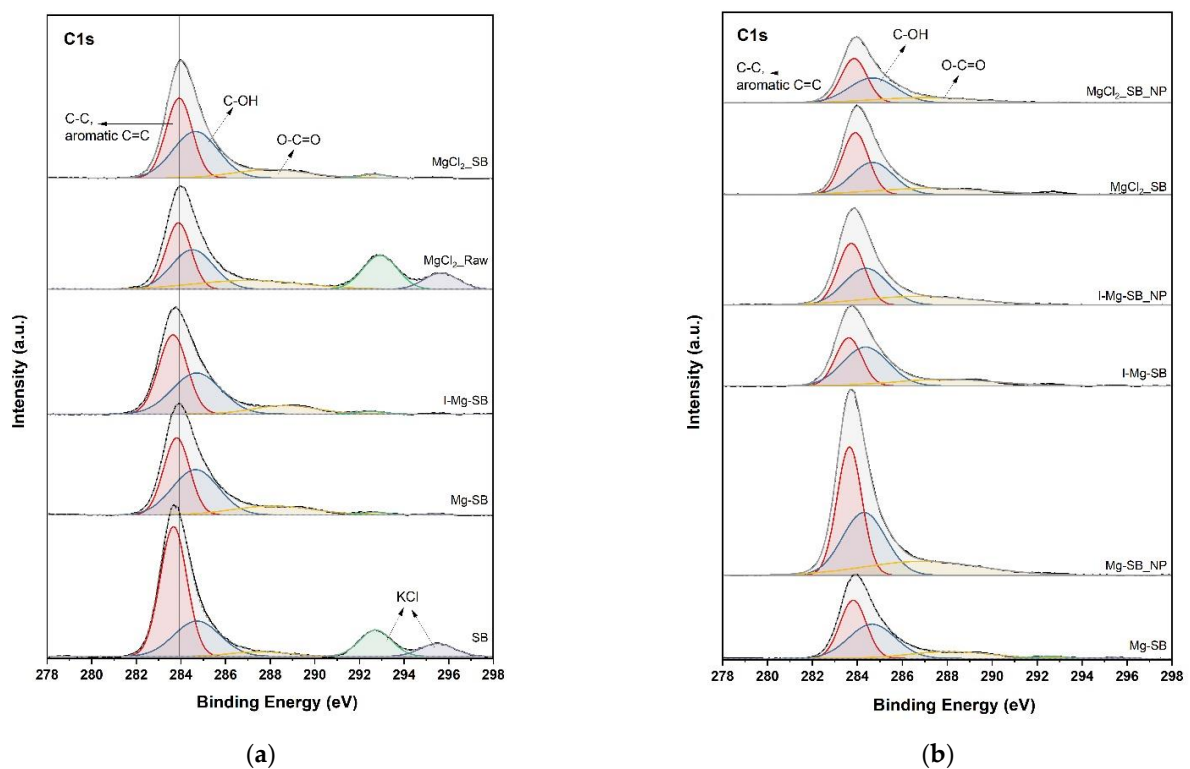


Figure 9. Cont.

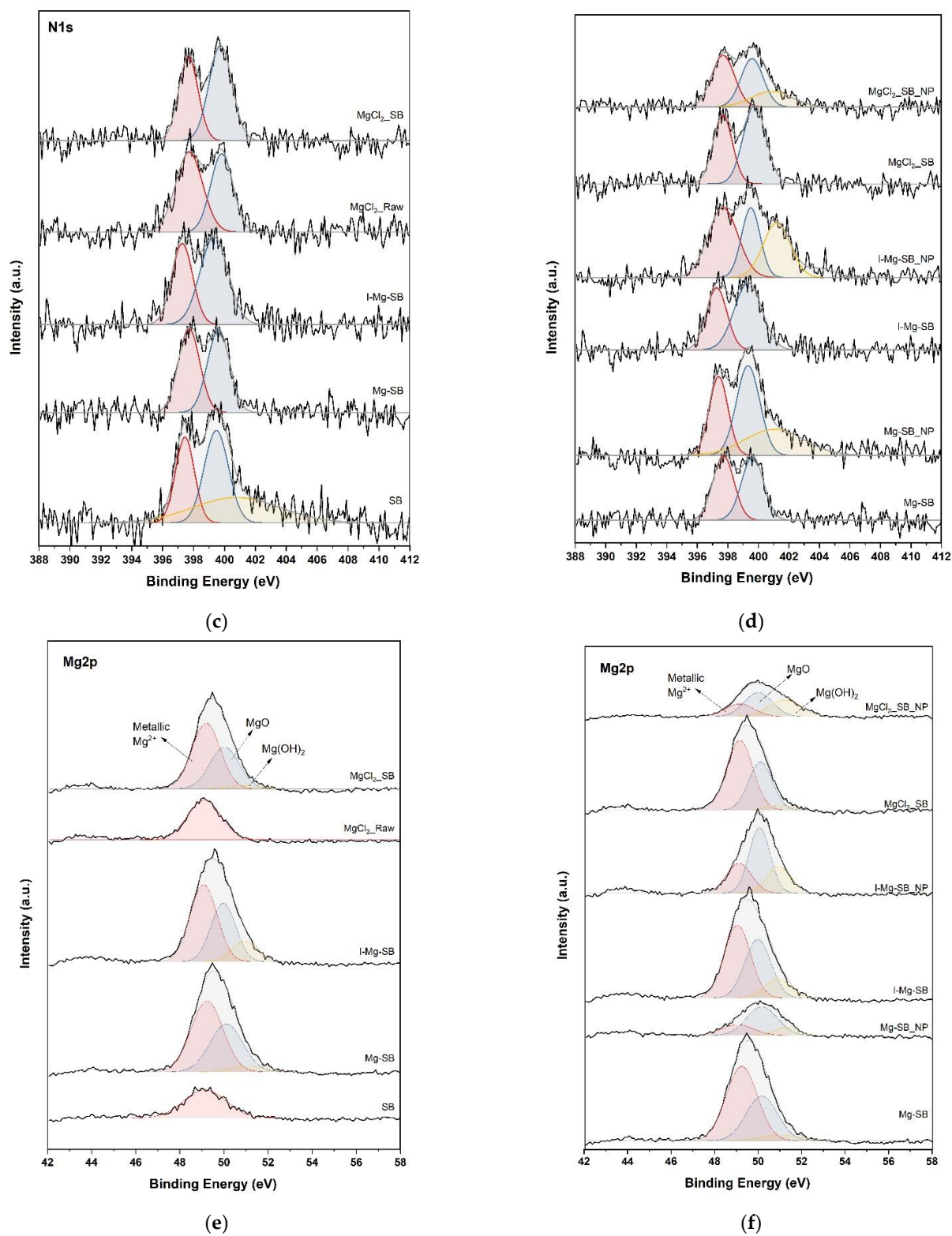


Figure 10. Cont.

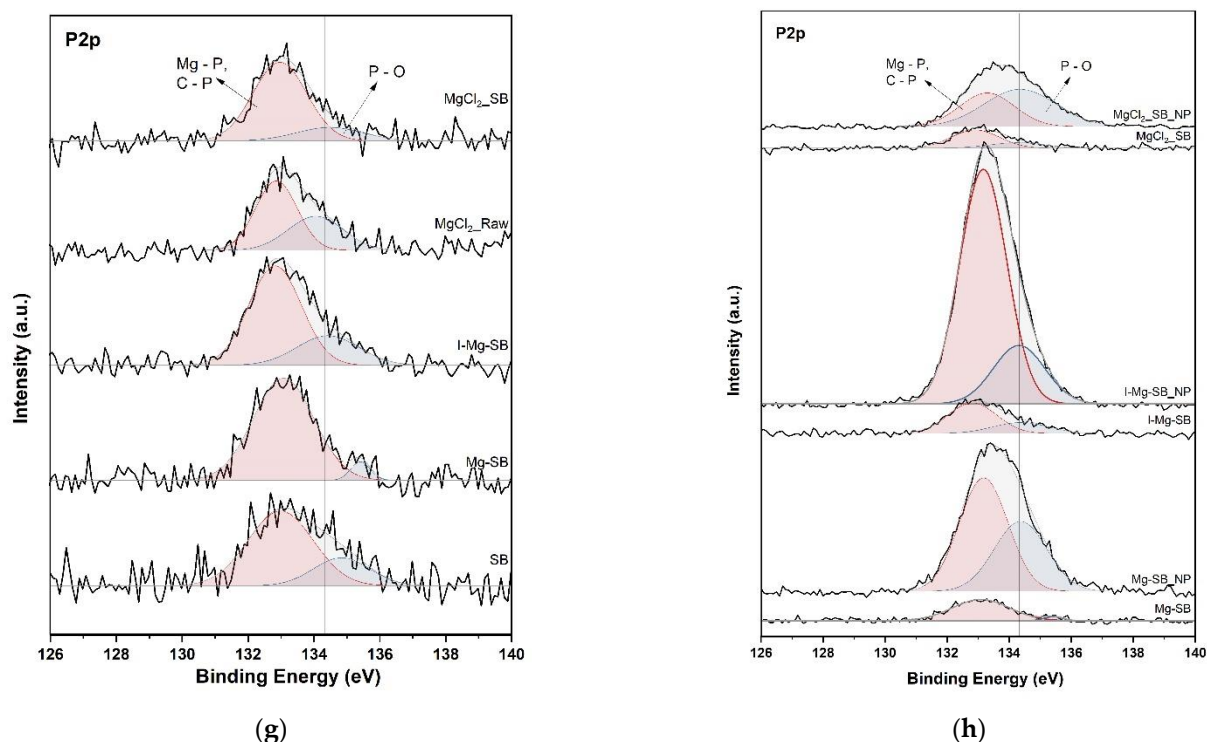


Figure 10. XPS spectra of C1s (a,b), N1s (c,d), Mg2p (e,f), and P2p (g,h) of biochar with different modification methods (a,c,e,g) and nutrient adsorptions (b,d,f,h).

The N1s graph confirms that the water leaching modification had no significant effect on the nitrogen functional groups. However, the inorganic nitrogen (ammonium) peaks of raw biochar at 401–402 eV [29,31] disappeared after the water treatment, and peaks did not appear for MgCl₂-Raw. The addition of MgCl₂ during pyrolysis may enhance the decomposition of ammonium-containing organic substances. The ammonium peak intensity after nutrient sorption varied in line with the removal rates.

The Mg2p graph in Figure 10 shows that peaks of MgO and Mg(OH)₂ were formed after the water leaching modification, and the peak intensity of metallic Mg²⁺ also increased. This result indicates that the Mg²⁺ eluted in the water leaching process was adsorbed to the biochar or converted to MgO or Mg(OH)₂. After the adsorption experiment, it was confirmed that the peak intensity of metallic Mg²⁺ was significantly reduced, indicating that the Mg²⁺-adsorbed biochar surface is involved in nutrient adsorption and crystallization.

In the case of P2p, the impact of different water leaching modification methods was negligible, but the P2p intensity increased significantly after nutrient adsorption. The Mg-P and C-P binding peaks of Mg-SB and I-Mg-SB increased considerably, suggesting that phosphate adsorption was associated with Mg as well as with biochar. Before the nutrient sorption test (Figure 10h), the Mg-P and C-P binding peak energies were lower than those after sorption. The peak shifted to a higher energy after the sorption test, suggesting that Mg-P binding was the main cause because most of the phosphates combined with Mg crystallized. In contrast, the peak at a lower binding energy before the sorption test could be interpreted primarily as an effect of C-P bonds. For MgCl₂-SB, PO₄ seemed to be removed independently from biochar by combining it with dissolved Mg²⁺. The lower phosphate removal efficiency of MgCl₂-SB, compared to that of Mg-SB and I-Mg-SB, which tended to be linked with biochar nutrient adsorption, stemmed from this different elimination mechanism. This showed that water leaching modification is more effective for sufficient nutrient sorption.

4. Conclusions

In this study, pyrolyzed SB, which has a high Mg content, was demineralized through water leaching, and simultaneously, eluted innate Mg was doped onto the biochar surface for PO₄ and NH₄ recovery. The CEC of SB increased as the pyrolysis temperature increased. In the process of water leaching, it was confirmed through XRD and XPS that aromatic carbon and carboxyl groups were involved in the adsorption of eluted Mg; therefore, MgO and Mg(OH)₂ were formed, and NaCl and KCl were removed. The nutrient sorption test showed 99% removal efficiency of PO₄ in a 600 ppm solution and only 5–15% removal efficiency for NH₄. The sample size of the adsorption experiment is a limitation, and the results of this paper may show relative tendencies, but there is insufficient statistical verification, so further research is needed for statistical verification. Competition between NH₄ and abundant K and Na ions was a factor for the low removal efficiency. For practical applications, further research on nutrient behavior, including the leaching tendency of nutrients, needs to be conducted. The ion exchange method after water leaching and pyrolysis was attempted by adding MgCl₂ to enhance the nutrient adsorption efficiency; ion exchange did not show a significant change and the adsorption efficiency of the MgCl₂-SB remained rather low, even though the Mg content was increased. The Mg2p XPS results of Mg-SB suggest that metallic Mg²⁺ adsorbed onto biochar is mostly utilized for nutrient adsorption. However, in the case of MgCl₂-SB, Mg did not react with the nutrients and formed Mg(OH)₂; therefore, the adsorption efficiency decreased. Further research is required to increase the adsorption efficiency of ammonium ions, but water leaching modification is a very effective method of upcycling SB for Mg surface doping and PO₄ adsorption.

Supplementary Materials: The following are available online at <https://www.mdpi.com/article/10.3390/su132212752/s1>, Figure S1: Electric furnace system for the pyrolysis experiment.

Author Contributions: Conceptualization, Y.-E.L.; Validation, Y.-E.L., Y.J. and I.-T.K.; Formal Analysis, Y.-E.L. and Y.J.; Data Curation, Y.-E.L., Y.J. and D.-C.S.; Investigation, Y.-E.L.; Resources, D.-C.S., K.-H.A. and J.-H.J.; Visualization, Y.-E.L.; Project Administration, Y.-E.L., Y.J. and D.-C.S.; Writing—Original Draft Preparation, Y.-E.L.; Writing—Review and Editing, Y.-E.L., Y.J. and I.-T.K.; Supervision, I.-T.K. All authors have read and agreed to the published version of the manuscript.

Funding: This work was financially supported by the Korea Institute of Civil Engineering and Building Technology (KICT), grant number 2021-0105.

Institutional Review Board Statement: Not applicable.

Informed Consent Statement: Not applicable.

Data Availability Statement: Not applicable.

Conflicts of Interest: The authors declare no conflict of interest.

References

1. Bird, M.I.; Wurster, C.M.; de Paula Silva, P.H.; Bass, A.M.; De Nys, R. Algal biochar—production and properties. *Bioresour. Technol.* **2011**, *102*, 1886–1891. [[CrossRef](#)]
2. Roberts, D.A.; Paul, N.A.; Dworjanyn, S.A.; Bird, M.I.; De Nys, R. Biochar from commercially cultivated seaweed for soil amelioration. *Sci. Rep.* **2015**, *5*, 9665. [[CrossRef](#)]
3. Poo, K.M.; Son, E.B.; Chang, J.S.; Ren, X.; Choi, Y.J.; Chae, K.J. Biochars derived from wasted marine macro-algae (*Saccharina japonica* and *Sargassum fusiforme*) and their potential for heavy metal removal in aqueous solution. *J. Environ. Manag.* **2018**, *206*, 364–372. [[CrossRef](#)] [[PubMed](#)]
4. Park, S.H.; Cho, H.J.; Ryu, C.; Park, Y.K. Removal of copper (II) in aqueous solution using pyrolytic biochars derived from red macroalga *Porphyra tenera*. *J. Ind. Eng. Chem.* **2016**, *36*, 314–319. [[CrossRef](#)]
5. Jung, K.W.; Kim, K.; Jeong, T.U.; Ahn, K.H. Influence of pyrolysis temperature on characteristics and phosphate adsorption capability of biochar derived from waste-marine macroalgae (*Undaria pinnatifida* roots). *Bioresour. Technol.* **2016**, *200*, 1024–1028. [[CrossRef](#)]
6. Mehta, C.M.; Khunjar, W.O.; Nguyen, V.; Tait, S.; Batstone, D.J. Technologies to recover nutrients from waste streams: A critical review. *Crit. Rev. Environ. Sci. Technol.* **2015**, *45*, 385–427. [[CrossRef](#)]

7. Rahman, M.M.; Salleh, M.A.M.; Rashid, U.; Ahsan, A.; Hossain, M.M.; Ra, C.S. Production of slow release crystal fertilizer from wastewaters through struvite crystallization—A review. *Arab. J. Chem.* **2014**, *7*, 139–155. [[CrossRef](#)]
8. Kim, D.; Ryu, H.D.; Kim, M.S.; Kim, J.; Lee, S.I. Enhancing struvite precipitation potential for ammonia nitrogen removal in municipal landfill leachate. *J. Hazard. Mater.* **2007**, *146*, 81–85. [[CrossRef](#)]
9. Nelson, N.O.; Mikkelsen, R.L.; Hesterberg, D.L. Struvite precipitation in anaerobic swine lagoon liquid: Effect of pH and Mg: P ratio and determination of rate constant. *Bioresour. Technol.* **2003**, *89*, 229–236. [[CrossRef](#)]
10. Zheng, W.; Sharma, B.K.; Rajagopalan, N. Using Biochar as a Soil Amendment for Sustainable Agriculture. Waste Utilization-Biochar. 2010. Available online: <http://hdl.handle.net/2142/25503> (accessed on 10 September 2021).
11. Zeng, Z.; Zhang, S.; Li, T.Q.; Zhao, F.L.; He, Z.L.; Zhao, H.P.; Yang, X.E.; Wang, H.L.; Zhao, J.; Rafiq, M.T. Sorption of ammonium and phosphate from aqueous solution by biochar derived from phytoremediation plants. *J. Zhejiang Univ. Sci. B* **2013**, *14*, 1152–1161. [[CrossRef](#)]
12. Zhang, M.; Gao, B.; Yao, Y.; Xue, Y.; Inyang, M. Synthesis of porous MgO-biochar nanocomposites for removal of phosphate and nitrate from aqueous solutions. *Chem. Eng. J.* **2012**, *210*, 26–32. [[CrossRef](#)]
13. Muhmood, A.; Lu, J.; Kadam, R.; Dong, R.; Guo, J.; Wu, S. Biochar seeding promotes struvite formation, but accelerates heavy metal accumulation. *Sci. Total Environ.* **2019**, *652*, 623–632. [[CrossRef](#)]
14. Kim, H.S.; Sanjeewa, K.K.; Fernando, I.P.; Ryu, B.; Yang, H.W.; Ahn, G.; Kang, M.C.; Heo, S.; Je, J.; Jeon, Y. A comparative study of *Sargassum horneri* Korea and China strains collected along the coast of Jeju Island South Korea: Its components and bioactive properties. *Algae* **2018**, *33*, 341–349. [[CrossRef](#)]
15. Sanjeewa, K.K.A.; Fernando, I.P.S.; Kim, E.A.; Ahn, G.; Jee, Y.; Jeon, Y.J. Anti-inflammatory activity of a sulfated polysaccharide isolated from an enzymatic digest of brown seaweed *Sargassum horneri* in RAW 264.7 cells. *Nutr. Res. Pract.* **2017**, *11*, 3–10. [[CrossRef](#)]
16. Lehmann, J.; Joseph, S. Biochar for environmental management: An introduction. In *Biochar for Environmental Management*, 2nd ed.; Routledge: London, UK, 2015; pp. 33–46.
17. Lee, Y.E.; Jo, J.H.; Kim, I.T.; Yoo, Y.S. Influence of NaCl concentration on food-waste biochar structure and templating effects. *Energies* **2018**, *11*, 2341. [[CrossRef](#)]
18. Kumar, P.S.; Korving, L.; Keesman, K.J.; van Loosdrecht, M.C.; Witkamp, G.J. Effect of pore size distribution and particle size of porous metal oxides on phosphate adsorption capacity and kinetics. *Chem. Eng. J.* **2019**, *358*, 160–169. [[CrossRef](#)]
19. Wang, C.C.; Hao, X.D.; Guo, G.S.; Van Loosdrecht, M.C.M. Formation of pure struvite at neutral pH by electrochemical deposition. *Chem. Eng. J.* **2010**, *159*, 280–283. [[CrossRef](#)]
20. Tansel, B.; Lunn, G.; Monje, O. Struvite formation and decomposition characteristics for ammonia and phosphorus recovery: A review of magnesium-ammonia-phosphate interactions. *Chemosphere* **2018**, *194*, 504–514. [[CrossRef](#)]
21. Chan, K.Y.; Xu, Z. Biochar: Nutrient properties and their enhancement. In *Biochar for Environmental Management*, 1st ed.; Routledge: London, UK, 2012; pp. 99–116.
22. Verheijen, F.; Jeffery, S.; Bastos, A.C.; Van der Velde, M.; Diafas, I. Biochar application to soils. In *A Critical Scientific Review of Effects on Soil Properties, Processes, and Functions*; JRC European Commission: Luxembourg, 2010; Volume 24099, p. 162.
23. Lehmann, J.; Rillig, M.C.; Thies, J.; Masiello, C.A.; Hockaday, W.C.; Crowley, D. Biochar effects on soil biota—A review. *Soil Biol. Biochem.* **2011**, *43*, 1812–1836. [[CrossRef](#)]
24. Stoch, J.; Ladecka, M. An XPS study of the KCl surface oxidation in oxygen glow discharge. *Appl. Surf. Sci.* **1988**, *31*, 426–436. [[CrossRef](#)]
25. Lu, H.; Zhang, W.; Yang, Y.; Huang, X.; Wang, S.; Qiu, R. Relative distribution of Pb²⁺ sorption mechanisms by sludge-derived biochar. *Water Res.* **2012**, *46*, 854–862. [[CrossRef](#)]
26. Shafeeyan, M.S.; Daud, W.M.A.W.; Houshmand, A.; Shamiri, A. A review on surface modification of activated carbon for carbon dioxide adsorption. *J. Anal. Appl. Pyrolysis* **2010**, *89*, 143–151. [[CrossRef](#)]
27. Boehm, H.P. Surface oxides on carbon and their analysis: A critical assessment. *Carbon* **2002**, *40*, 145–149. [[CrossRef](#)]
28. Singh, B.; Fang, Y.; Cowie, B.C.; Thomsen, L. NEXAFS and XPS characterisation of carbon functional groups of fresh and aged biochars. *Org. Geochem.* **2014**, *77*, 1–10. [[CrossRef](#)]
29. Wei, L.; Hong, T.; Li, X.; Li, M.; Zhang, Q.; Chen, T. New insights into the adsorption behavior and mechanism of alginate acid onto struvite crystals. *Chem. Eng. J.* **2019**, *358*, 1074–1082. [[CrossRef](#)]
30. Shi, Q.; Zhang, H.; Shahab, A.; Zeng, H.; Zeng, H.; Nabi, I.; Siddique, J.; Ullah, H. Efficient performance of magnesium oxide loaded biochar for the significant removal of Pb²⁺ and Cd²⁺ from aqueous solution. *Ecotoxicol. Environ. Saf.* **2021**, *221*, 112426. [[CrossRef](#)] [[PubMed](#)]
31. Gong, B.; Pigram, P.J.; Lamb, R.N. Identification of inorganic nitrogen in an Australian bituminous coal using X-ray photoelectron spectroscopy (XPS) and time-of-flight secondary ion mass spectrometry (TOFSIMS). *Int. J. Coal Geol.* **1997**, *34*, 53–68. [[CrossRef](#)]